EDMS No. 404386

ORGANISATION EUROPEENNE POUR LA RECHERCHE NUCLEAIRE
EUROPEAN ORGANIZATION FOR NUCLEAR RESEARCH

Laboratoire Européen pour la Physique des Particules
European Laboratory for Particle Physics

Technical Inspection and Safety Division

Technical Note
CERN-TIS-2003-017-RP-TN

Parameters of radiological interest for a beta-beam decay ring

M. Magistris[(1)] and M. Silari

[(1)] Fellow in AB Division

Abstract

In a beta-beam facility, a pure beam of electron neutrinos or their antiparticles is produced through the decay of fully stripped radioactive ions (^{6}He and ^{18}Ne) circulating in a storage ring. Since the beam is not extracted from the ring, all the particles will eventually be lost somewhere in the machine and thus activate the machine components and the surrounding concrete and rock. In particular, as nuclei change their charge in beta-decay, a large part of the particles will be lost in the arcs of the decay ring and mainly irradiate the magnets. The density of inelastic interactions of hadrons in the magnets, concrete and rock and the track-length distribution of secondary hadrons were calculated by means of the FLUKA Monte Carlo code. These values were used to estimate the induced radioactivity in the facility, the dose rates expected in the decay ring and the consequences for the environment.

CERN, 1211 Geneva 23, Switzerland
22 September 2003

1. Introduction

In a Beta-beam facility, a pure beam of electron neutrinos or their antiparticles is produced through the decay of radioactive ions circulating in a storage ring [Lin02]. At present, ^{6}He and ^{18}Ne are being considered. The beta-emitting radioactive ions will be produced in an particle separator on-line (ISOL) system using the proposed Superconducting Proton Linac (SPL) as a driver [Bon02]. The ion beam is first accelerated in two cyclotrons and then transferred to the Proton Synchrotron (PS) and Super Proton Synchrotron (SPS) for further acceleration. As they reach their final kinetic energy (139 GeV/u for ^{6}He and 55 GeV/u for ^{18}Ne) the ions are stored in a decay ring, where they decay emitting electron neutrinos.

Since no beam is ejected from the ring, these particles will eventually be lost somewhere in the machine and thus activate the magnets and the surrounding concrete and rock. Beam-gas interactions of the ions circulating in the ring will also contribute to beam losses and thus to material activation. The cascades induced by the lost particles have been simulated by the Monte Carlo code FLUKA [Fas00a, Fas00b]. This paper describes the determination of parameters of radiological interest (residual nuclei, star density, particle tracklength) normalized to a loss of one particle per metre [Ste92]. Finally, these parameters are applied to a specific possible configuration of the decay ring [Lin02], to obtain the dose rates expected during maintenance and the consequences for the environment.

2. The decay ring and beam losses

A possible layout of the decay ring is shown in figure 1. The ring consists of two straight sections and two bending sections (arcs). The straight sections are supposed to be 2,500 m long; the length of the arcs depends on the dipole design. Because electron neutrinos from ions decaying in the arcs cannot be collected and used for experiments, the neutrino-production efficiency depends on the arc length versus straight section length. A strong magnetic field in the magnets would allow using short arcs and therefore obtaining good neutrino-production efficiency in the decay ring. In the proposed scenario [Lin02], the arcs have a radius of 300 m.

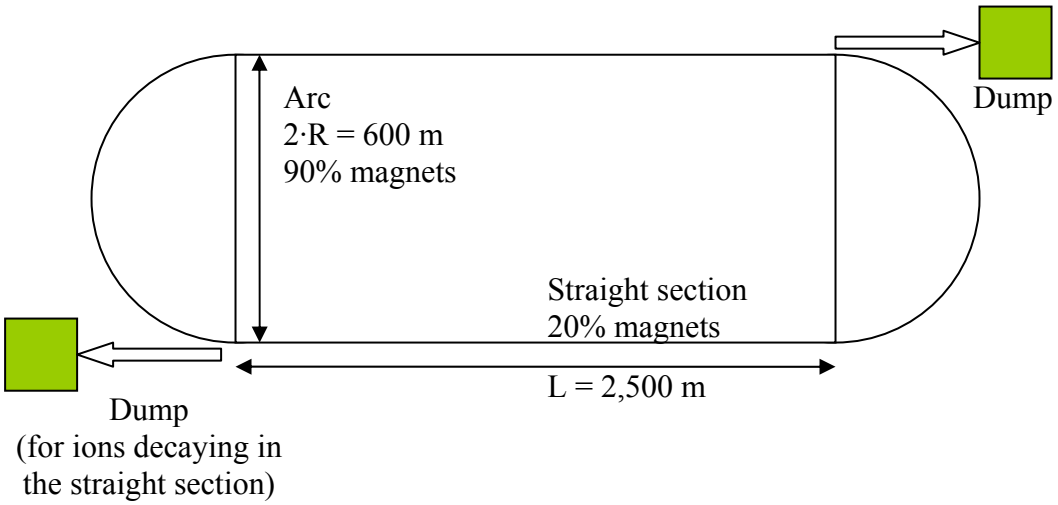

Figure 1. A possible layout of the decay ring.

Losses in the decay ring can be estimated using the fact that the beam is not extracted and thus all injected beam is essentially lost somewhere in the machine. The beam power lost in the ring during operation is supposed to be 157 kW for ^{6}He and 10.6 kW for ^{18}Ne [Lin02]. With the proposed scenario and assuming that the ions decay uniformly in the ring, 14% of the ions decay in each arc and 36% in

each straight section. The ions change their charge in the decay: beta decay products have a different trajectory in the magnets with respect to the parent radioactive ions and thus are lost. This leads to a uniformly distributed power deposit in each arc of 21.980 kW for ^{6}He (i.e., 23.3 W m^{-1}) and 1.484 kW for ^{18}Ne (i.e., 1.57 W m^{-1}). In this report, by 'standard conditions' we mean ^{6}He and ^{18}Ne beams circulating simultaneously and uniformly-distributed beam losses in the arcs of 23.3 W m^{-1} and 1.57 W m^{-1} for ^{6}He and ^{18}Ne, respectively. Ions decaying in a straight section end up in a dump placed downstream of the first bend. Such dump copes with a beta-decay product beam of 56 kW for ^{6}He and 3.8 kW for ^{18}Ne parent ions.

In both arcs and straight sections, some ions interact with the residual gas in the vacuum chamber. Even if a good estimate of the beam-gas interactions requires a detailed study, in a first approximation one can use expression (1) below suggested by Eggert [Ste92] for estimating the beam-gas proton loss rate in one ring of the LHC:

$$\frac{dN}{dt} = -\frac{1}{\tau_g} N, \qquad (1)$$

where N is the number of particles circulating in the ring and τ_g is the life-time of the beam due to beam-gas interactions which is equal to $1/(\rho \cdot \sigma_{tg} \cdot c)$, where ρ is the sum of the number densities (i.e., the number of atoms per unit volume) of carbon and oxygen atoms in the residual gas, σ_{tg} is the total particle-gas cross-section and c is the velocity of light. In the following analysis, in order to have a first approximation of the rate of particle loss, we assume that a nucleus of ^{6}He (^{18}Ne) will interact with a molecule of gas with the same probability of 6 (18) single protons; that is, a total cross-section of 465 mbarn is taken for σ_{tg} [Ste92]. The equivalent oxygen atom density expected in the vacuum system is assumed to be $9.5 \cdot 10^{7}$ atoms per cubic centimeter, as in the LHC vacuum system [Ste92]. According to this analysis, the life-time of the beam is $7.5 \cdot 10^{5}$ s, a value which is extremely high if compared with the half-life of ^{6}He (0.80 s). For this reason, in the arcs beam-gas losses are negligible with respect to decay losses. However, before inferring that beam-gas losses are also negligible in the straight sections, where fewer decay products are deposited, one should estimate the number of beam-gas interactions per second. According to expression (1), beam-gas losses are proportional to the number N of ions circulating in the ring, that is $2.0 \cdot 10^{14}$ ions of ^{6}He and $9.1 \cdot 10^{12}$ ions of ^{18}Ne [Lin02][1]. The number of beam-gas interactions is thus $2.66 \cdot 10^{8}$ s^{-1} (34 W, 4.9 mW m^{-1}) for ^{6}He and $1.21 \cdot 10^{7}$ s^{-1}

[1] The value N may be calculated from the lost power (^{6}He: 157 kW, ^{18}Ne: 10.6 kW) in the ring, the ion mean lifetime at rest (^{6}He: 0.8/log2 s, ^{18}Ne: 1.67/log2 s) and the rest energy per ion (Lorentz gamma of ^{6}He: 150, ^{18}Ne: 60) using expression (2) [Jan03]:

$$< power\ lost > = \frac{< rest\ energy\ per\ ion > \cdot < number\ of\ stored\ ions >}{< decay\ time\ at\ rest >} \qquad (2)$$

which for ^{6}He and ^{18}Ne leads to expressions (3) and (4), respectively:

$$157{,}000\, W = \frac{\frac{(139 \cdot 10^{9}\ eV) \cdot 6}{150} \cdot (1.6 \cdot 10^{-19}\ \frac{J}{eV}) \cdot N_{6He}}{\frac{0.8\ s}{\log 2}} \qquad (3)$$

$$10{,}600\, W = \frac{\frac{(55 \cdot 10^{9}\ eV) \cdot 18}{60} \cdot (1.6 \cdot 10^{-19}\ \frac{J}{eV}) \cdot N_{18Ne}}{\frac{1.67\ s}{\log 2}} \qquad (4)$$

From these data, one obtains ~$2.0 \cdot 10^{14}$ ions of ^{6}He and ~$9.6 \cdot 10^{12}$ ions of ^{18}Ne stored in the ring, values which are consistent, within the rounding errors, to those estimated in [Lin02].

(1.91 W, 0.3 mW m^{-1}) for ^{18}Ne. Under the assumptions made for estimating the beam life-time, beam-gas losses give a contribution to the material activation which is three orders of magnitude lower than the contribution of decay losses. In the following chapters, beam-gas losses will thus be neglected in the calculations of the induced radioactivity in the magnets and vacuum chambers of the arcs and in the concrete wall and rock. Star densities per unit lost power in magnets and vacuum chambers due to beam-gas interactions are provided for completeness, in case more accurate values of gas density will in the future lead to a different beam life time, and for estimating the dose rates expected in the straight sections, where no contribution to material activation is supposed to come from decay losses.

3. FLUKA simulations

For this preliminary study of the material activation, magnets and vacuum chambers in the decay ring of a Beta-beam facility are assumed to be similar to those of the main ring of the Large Hadron Collider (LHC), as suggested by Lindroos [Lin03]. Because at the present design stage there is no detailed layout of the ring, the same simplified geometrical models for the LHC main ring [Ste02] were used in these simulations. In particular, different simulations were run for two possible configurations: a tunnel with a vacuum chamber inside a magnet, and a tunnel with a vacuum chamber only. In the former model the vacuum chamber plus magnet were represented by an iron cylinder of 2 cm inner radius and 20 cm thickness, placed at the centre of a cylindrical tunnel of 1.8 m radius. A concrete wall-thickness of 30 cm was assumed and the tunnel was embedded in a 270 cm thick layer of rock. In the latter model, the magnet was replaced by a vacuum chamber of the same internal radius and of 2.2 cm outer radius, also made of iron. A total length of 50 m was assumed in both simulations.

Experimental data on neutron emission from the interaction of heavy ion beams with matter are far less abundant than data on neutron production from protons. In addition the generalized Monte Carlo codes applicable for radiation protection calculations, such as FLUKA, MCNPX [Pra89] and MARS [Mok98], do not generally treat secondary particle production from ions with masses larger than one atomic mass unit. Development work is under way to implement ion transport in both FLUKA and MARS, but the new versions of the codes have not yet been released. In FLUKA ion transport above a few GeV is well advanced [And02], and a model to transport ions down to energy of about 50 MeV per nucleon is presently under implementation.

Measurements of the spectral fluence and the ambient dose equivalent of secondary neutrons produced by 250 GeV/c protons and 158 GeV/c per nucleon lead ions were performed at CERN around a thick beam dump [Ago01]. These measurements showed that the spectral fluence of the secondary neutrons outside a thick shield is similar for light (protons) and heavy (lead) ions of comparable energy per nucleon stopped in a thick target [Ago02]. Because a great contribution to star density production and material activation come from secondary neutrons, this model has been applied to estimate the induced radioactivity in the decay ring. In particular, 139 GeV/u ^{6}He ions were simulated as a group of 6 independent 139 GeV protons, and 55 GeV/u ^{18}Ne ions as 18 independent 55 GeV protons.

In order to simulate interactions of beta-decay products, a 139 GeV (55 GeV) proton beam was sent onto the inner surface of the magnet (or the vacuum chamber) with an angle of incidence of 1 deg. Beam-gas interactions were simulated by filling the vacuum chamber with graphite and sending the proton beam into the system on the axis of the cylinders at a depth of 5 m. This ensured that all protons interacted in the system and that the cascade would be completely developed within the dimensions of the simulations. The longitudinal development of the cascade is shortened and secondary interactions which might have taken place in the coils of the magnet in the real case will rather occur in the graphite in the simulations. However, since one is mainly interested in longitudinally integrated parameters near the outer part of the magnet, this and the lateral attenuation provided by the graphite should not affect the results to a significant extent [Ste92].

Because only hadronic interactions are of interest in the present study, electrons, photons and neutrinos were discarded. Hadrons were transported down to 50 MeV, except neutrons, which were followed down to the thermal range (<0.41 eV). To improve calculation efficiency, a survival probability factor of 0.7 was applied for neutron collisions below 0.1 MeV. Because the total length of all magnets is about 90% of the length of the arcs (20% of the length of the straight sections), quantities of radiological interest in the air and rock can be estimated by taking 9/10 of the appropriate quantity estimated from the 'with-magnet' simulations for the arcs (2/10 for the straight sections) and 1/10 (8/10) of the same quantity estimated from the 'without-magnet' simulation.

4. Inelastic-interaction scoring

The spatial distribution of the number of stars (inelastic interactions of hadrons having kinetic energies greater than 50 MeV) was recorded in the form of star density distributions in cylindrical bin structures and as the total numbers of stars occurring in the different regions. The number of stars scored with FLUKA per single proton was multiplied by 6 (18) to obtain the number of stars produced by a nucleus of ^{6}He (^{18}Ne); the results are shown in table 1. As already mentioned magnet, vacuum chamber, concrete wall and rock shield were given a length of 50 m in order to absorb the whole hadronic cascade. However, because the vacuum chamber is thin (2 mm) when compared to the magnets (20 cm) and due to the high energy and little angle of incidence (1 deg) of the beam, only a fraction of the secondary particles (30.4% in the case of ^{6}He, 39.1% in the case of ^{18}Ne) were actually deposited in the components. Because the radial distribution of stars produced by beam particles striking the vacuum chamber strongly depends on the longitudinal distance from the point of interaction, the definition of an average radial distribution requires some assumptions. Here it was assumed that all secondary particles generated by particles striking the vacuum chamber and escaping the system would be absorbed in the concrete wall and in the surrounding rock with an average radial distribution which is similar to the average over the first 50 m length only. Because only 30.4% and 39.1% of the secondary particles produced by ^{6}He and ^{18}Ne, respectively, were actually deposited in the simulated geometry (i.e., vacuum chamber and surrounding concrete and rock), values found with FLUKA relative to concrete and rock were normalized to the total number of secondary particles produced (i.e., they were multiplied by a factor 1/0.304 and 1/0.391 for ^{6}He and ^{18}Ne, respectively). Because only ~10% of the arcs of the decay ring will be without magnets, small discrepancies from the values found with this simplified model should not have severe consequences on the final results.

Table 1. Inelastic interactions per primary ion scored in the components of the decay ring due to decay losses. Values in rows labeled with 'm.' refer to sections with vacuum chamber and magnet, values in rows labeled with 'v.c.' refer to sections without magnets (vacuum chamber only). π are charged pions. The total is the sum of the three previous columns plus all other secondary particles.

Inelastic interactions (stars) per primary ion (decay losses)								
	^{6}He, E_{kin}=834 GeV				^{18}Ne, E_{kin}=990 GeV			
	π	p	n	Total	π	p	n	Total
Vacuum chamber	7.81	5.30	2.24	16.91	30.38	35.81	11.83	83.5
Magnet	417.6	165	785.4	1420.2	529.2	250	1079	1917
Concrete (v.c.)	327.8	123.1	477.4	939.76	447.9	198.4	723.2	1396
(m.)	18.34	10.44	196.8	226.8	23.76	15.04	270.9	311.4
Rock (v.c.)	56.18	29.21	383.8	472.1	81.48	46.91	586.5	719.5
(m.)	5.46	7.188	209.6	222.9	7.2	10	289.8	307.8

On average, ^{18}Ne particles generate more stars than ^{6}He, mainly because of their higher total kinetic energy. In the components close to the beam (e.g., vacuum chambers and magnets), pions and

protons strongly contribute to the star production; in the rock surrounding the facility, most of the inelastic interactions are due to neutrons. Table 2 shows the stars produced in the components of the ring per beam particle interacting with the residual gas. The number of inelastic interactions induced by a particle striking the magnet (or the vacuum chamber) is larger if the particle has full energy (table 1) and smaller if the particle has lost part of its energy by interactions with a molecule of gas (table 2). This is particularly true for ^{18}Ne, which has a lower kinetic energy per nucleon.

Table 2. Inelastic interactions per primary ion scored in the components of the decay ring, due to beam-gas interactions. Values in rows labeled with 'm.' refer to sections with vacuum chamber and magnet, values in rows labeled with 'v.c.' refer to sections without magnets (vacuum chamber only). π are charged pions. The total is the sum of the three previous columns plus all other secondary particles.

Inelastic interactions (stars) per primary ion (beam-gas interactions)								
	^{6}He, E_{kin}=834 GeV				^{18}Ne, E_{kin}=990 GeV			
	π	p	n	Total	π	p	n	Total
Vacuum chamber	11.94	3.34	4.2	21.42	14.76	5.382	6.44	28.6
Magnet	363.6	136.8	697.2	1236.6	473.4	199.8	964.8	1683
Concrete (v.c.)	292.8	119.4	457.8	889.2	390.6	178.4	649.8	1240.2
(m.)	17.46	10.08	179.4	208.2	23.04	14.4	247.6	286.2
Rock (v.c.)	56.34	30.48	376.8	466.8	76.68	45.9	534.6	660.6
(m.)	5.22	6.72	190.2	202.8	6.84	9.72	262.8	280.8

The longitudinally integrated star density rate in the magnet is given as a function of radius in table 3. The star density in this table is normalised to a beam loss of 1 W m^{-1}, i.e. the star density averaged over 50 m length has been normalised to one proton per metre and eventually multiplied by the number of nucleons per second striking the magnet per 1 W (^{6}He: 1 W ~ $4.49\cdot10^{7}$ nucleons s^{-1}; ^{18}Ne: 1 W ~ $1.13\cdot10^{8}$ nucleons s^{-1}).

Table 3. Star density rate in magnets per unit lost power (cm^{-3} s^{-1})/(W m^{-1}) for decay losses and beam-gas interactions, as a function of radius.

Radial star density rate (cm^{-3} s^{-1})/(W m^{-1}) in the magnets, decay losses.				
	1-5 cm	6-10 cm	11-15 cm	16-20 cm
^{6}He	$3.52\cdot10^{5}$	$8.98\cdot10^{4}$	$3.86\cdot10^{4}$	$1.93\cdot10^{4}$
^{18}Ne	$3.98\cdot10^{5}$	$1.01\cdot10^{5}$	$4.38\cdot10^{4}$	$2.20\cdot10^{4}$
Radial star density rate (cm^{-3} s^{-1})/(W m^{-1}) in the magnets, beam-gas interactions.				
^{6}He	$2.87\cdot10^{5}$	$8.23\cdot10^{4}$	$3.52\cdot10^{4}$	$1.77\cdot10^{4}$
^{18}Ne	$3.28\cdot10^{5}$	$9.43\cdot10^{4}$	$4.06\cdot10^{4}$	$2.04\cdot10^{4}$

Because of the different decay modes of ^{6}He (β^{-}) and ^{18}Ne (β^{+}), the decay products have a different trajectory in the dipoles. In particular, ^{6}He ions will be lost inwards whilst ^{18}Ne ions will be lost outwards with respect to the reference orbit. Although this feature may have some consequences on the distribution of induced radioactivity in the magnets, it has no noticeable effect on the induced radioactivity in the concrete wall and the surrounding rock, as shown in figure 2. The star density distribution in concrete and rock is thus only a function of the radial distance from the beam axis.

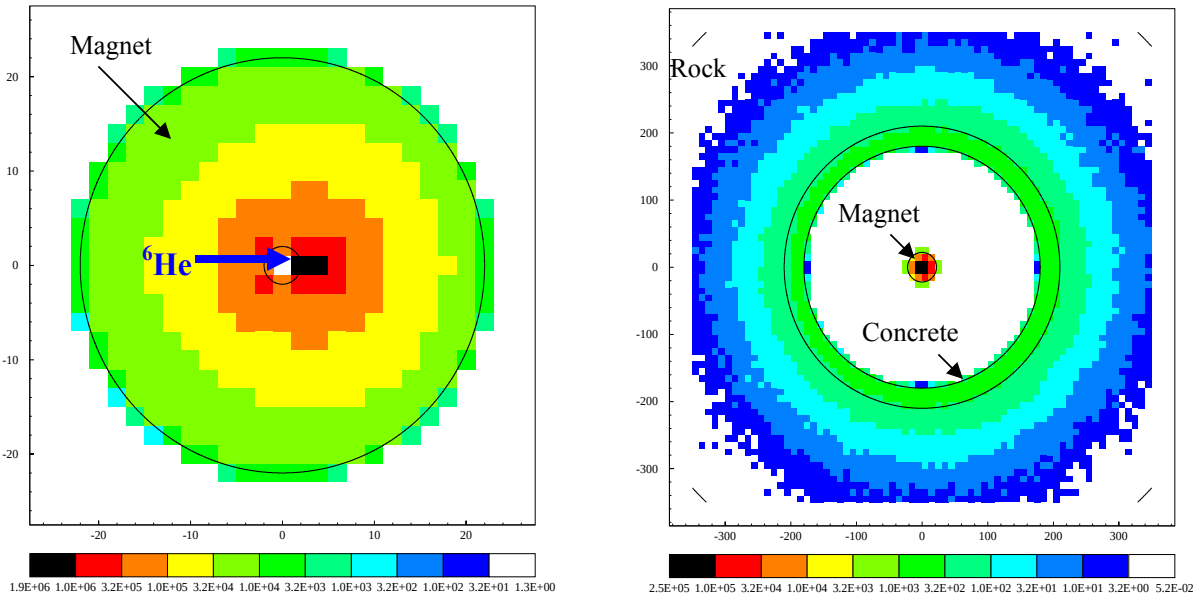

Figure 2. Star density rate per unit lost beam power (cm^{-3} s^{-1} W^{-1} m) of ^{6}He in magnets (left) and rock (right). Scales are in cm and colour scales are different in the two pictures.

The variation of the star density in the concrete and in the rock in the arcs is plotted in figures 3,4 as a function of radius. Data are presented for the simulations with and without magnets; the combined distribution (dashed line) of the two geometries is taken to represent the real situation. Ions lost in sections with vacuum chamber only give a higher contribution to the activation of the rock, if compared to sections with magnets. This happens because a magnet absorbs a larger part of the secondary particles with respect to a vacuum chamber.

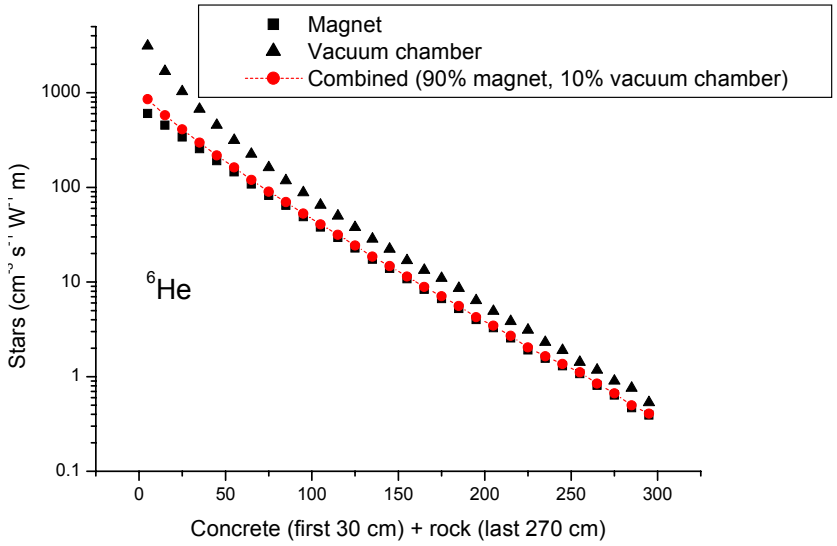

Figure 3. Star density rate per unit lost beam power of ^{6}He in the concrete and in the rock in the arcs as a function of radial distance from the beam axis.

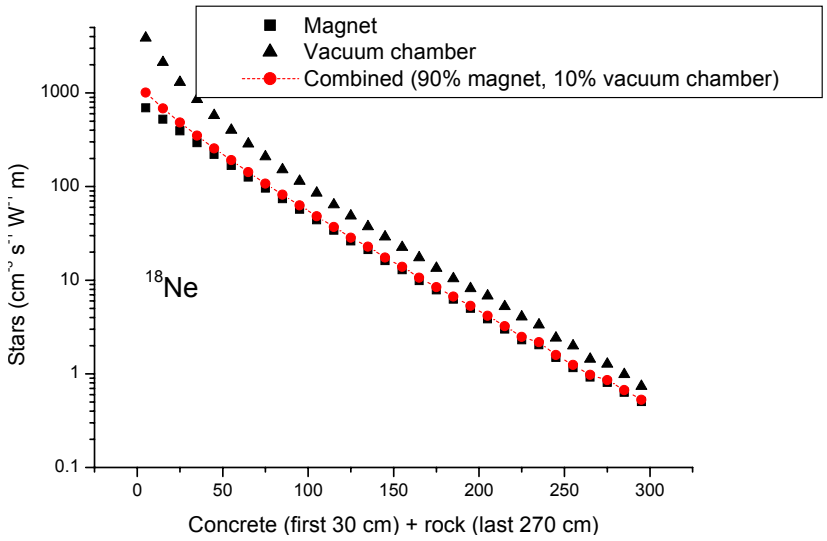

Figure 4. Star density rate per unit lost beam power of ^{18}Ne in the concrete and in the rock in the arcs as a function of radial distance from the beam axis.

Because heat deposition may affect the properties of the magnets, the deposited energy distribution in the arcs was studied with the USRBIN option of FLUKA. Figure 5 shows the distribution of ^{6}He and secondary particles deposited in the magnets of the arcs. Although in the inner layer the highest value of deposited energy (0.42 mW g^{-1}) is found inwards (i.e., right side of figure 5), particles are distributed in the outer layer with almost cylindrical symmetry.

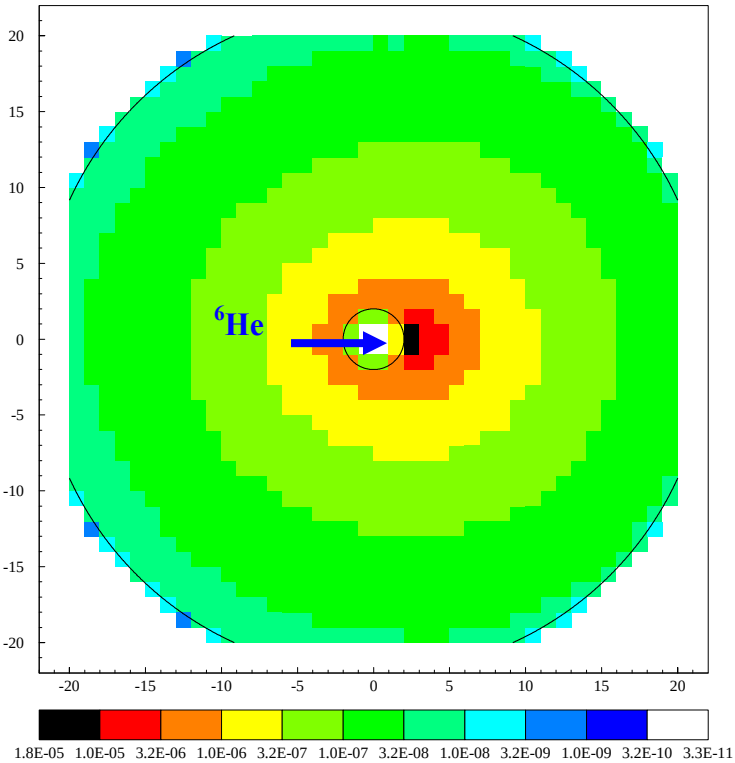

Figure 5. Deposited power per unit lost beam power (W g^{-1})/(W m^{-1}) by ^{6}He and secondary particles in the magnets of the arcs. Scales are in cm.

5. Induced radioactivity

The specific activity expected in the magnets after the shutdown of the facility increases linearly with increasing beam losses. The production rates of particles in iron were scored using the RESNUC option of FLUKA. The data were analysed by means of a specific program (rusrsuw) to obtain specific activities after an irradiation cycle consisting of 10 years of operation (6 month irradiation + 6 month decay each year), followed by different waiting times. The results are shown in table 4; contributions from different primary particles (^{6}He, ^{18}Ne) through different activation modes (decay losses, beam-gas interactions) are shown separately. One can also estimate the saturation activity in the magnets from the star production rate (tables 1 and 2) and the number of particles lost per second, averaged over 1 year of operation (i.e., the number of particles lost per second, divided by 365 days and multiplied by the number of days of operation per year). Neglecting the contribution of beam-gas interactions, this procedure leads to a saturation activity of 4,565 (Bq g^{-1})/(W m^{-1}) from ^{6}He and 5,118 (Bq g^{-1})/(W m^{-1}) from ^{18}Ne. These values, when compared to those of table 4, show that after 10 years of operation the induced radioactivity in the magnets is still relatively far from saturation. This means that the specific activity expected in the magnets strongly depends on the period of operation. Even 10 years after the shutdown of the facility, the induced radioactivity (~2,500 Bq g^{-1}) is above the Swiss Exemption Limits. These components should thus be disposed of as radioactive waste.

Table 4. Specific activity in the magnets per unit lost power (Bq g^{-1})/(W m^{-1}) after 10 years of operation, as a function of waiting time.

Specific activity (Bq g^{-1})/(W m^{-1}) in the magnets after 10 years of operation				
Waiting time	^{6}He (decay losses)	^{18}Ne (decay losses)	^{6}He (beam-gas)	^{18}Ne (beam-gas)
1 month	$2.38 \cdot 10^{3}$	$2.71 \cdot 10^{3}$	$2.13 \cdot 10^{3}$	$2.43 \cdot 10^{3}$
1 year	$1.26 \cdot 10^{3}$	$1.42 \cdot 10^{3}$	$1.12 \cdot 10^{3}$	$1.28 \cdot 10^{3}$
10 years	100	113	85.7	97.6
100 years	0.7	0.79	0.56	0.64

6. Dose rates

The star densitie rates in the outer layers of the magnets can be related to the dose rate using a so called ω-factor [Hoe75]. This factor converts the star production rate averaged over the outer 5 cm of a large object into the dose rate in contact with the object. For iron the ω-factor after 30-day irradiation and 1-day decay is $5.0 \cdot 10^{-6}$ mSv h^{-1} cm^{3} s. Multiplying the ω-factor by the values of table 3, one obtains the contact dose rate per unit lost power (table 5).

Table 5. Dose rates in contact with the magnets (after 30-day irradiation and 1-day decay) per unit lost power (mSv h^{-1})/(W m^{-1}), due to decay losses and beam-gas interactions.

	Contact dose rate (mSv h^{-1})/(W m^{-1})	
	Decay losses	Beam-gas interactions
^{6}He	0.10	0.09
^{18}Ne	0.11	0.10

As an example, under standard conditions after 30 days of continuous irradiation and 1 day waiting time the dose rate in contact with the magnets in the arcs is ~2.5 mSv h^{-1}. Although the dose rates strongly depend on the unit lost power (i.e., on the arc length), from this value one can conclude that any maintenance operation, if not remote-handled, must be carefully planned to reduce exposure to radiation. In the straight sections, if beam-gas interactions only are responsible for material activation, after 30-day irradiation and 1-day decay the dose rate in contact with the magnets is 0.4 μSv h^{-1} (^{6}He) and 0.03 μSv h^{-1} (^{18}Ne).

Because the ω-factors only apply to large objects, the dose rate expected at some distance from the vacuum chamber was estimated with the software package MicroShield [Mic96]. For a given source of radioactivity and a defined geometry, MicroShield calculates numerically the dose rate expected at a given point from the source, only taking into account photons from gamma-emitters (in particular, gammas produced by annihilation of positrons are not considered). The dose rates from the vacuum chamber, normalized to unit lost power, are shown in table 6; these values were estimated taking into account γ-emissions from ^{52}Mn, ^{48}V, ^{46}Sc and ^{54}Mn (particles contributing to 90% of the total energy emitted through gamma radiation). The ambient dose equivalent rate H*(10) expected at 10 cm from the vacuum chamber in the arcs after 30 days of irradiation and one day waiting is 1.5 mSv h^{-1}, under standard conditions. In the straight sections, if only beam-gas interactions are responsible for material activation, after 30-day irradiation and 1-day decay the dose rate in contact with the vacuum chamber is 0.4 μSv h^{-1} (^{6}He) and 0.03 μSv h^{-1} (^{18}Ne).

Table 6. H*(10) at 10 cm from the vacuum chamber (after 30-day irradiation and 1-day decay) per unit lost power (mSv h^{-1})/(W m^{-1}), due to decay losses and beam-gas interactions.

	Dose rate at 10 cm distance (mSv h^{-1})/(W m^{-1})	
	Decay losses	Beam-gas interactions
^{6}He	0.06	0.09
^{18}Ne	0.095	0.10

The dose rates expected in the arcs of the decay ring after 10 years of operation and one month waiting time, under standard conditions, were also calculated with MicroShield. Dose rates due to the concrete wall were calculated taking into account the specific activities of ^{22}Na and ^{7}Be (which are responsible for more than 95% of the gamma emissions) averaged over a 30 cm thick layer and combining the results of the configuration with and without magnets. The results are given in table 7; values are taken at one metre from the magnets and the vacuum chamber and at 10 cm from the wall. However, because the tunnel is long with respect to its diameter (942 m length, 3.6 m diameter), the dose rate due to the concrete only slightly depends on the distance from the wall. One month after the shutdown of the facility, the expected H*(10) is ≈0.8 mSv h^{-1} in sections with magnets and ≈0.2 mSv h^{-1} in sections without magnets.

Table 7. H*(10) (μSv h^{-1}) expected in the arcs of the decay ring, after 10 year operation and 1 month waiting time, under standard conditions. The dose rates due to the concrete wall were calculated combining the results of the configuration with and without magnets.

	Dose rate from concrete			Dose rate from magnets	Dose rate from vacuum chambers
	With magnets	Without magnets	Combined		
^{6}He	20	92	27.2	690	170
^{18}Ne	1.5	7.8	2.13	54	5.7
Total	29			744	176

7. Radioactivity in the rock

The decay ring is supposed to be built underground. The 30 cm thick concrete wall is surrounded by a thick layer of rock, which is assumed to be molasse (the typical rock of the Geneva area). In this section attention will be restricted to the rock surrounding the arcs and to those nuclides that have actually been detected and measured in the molasse at CERN [Ren83, Sul87]. Most of these particles are produced by spallation. However, the europium nuclides are produced by the absorption of thermal neutrons. Nevertheless, the experimental data of Sullivan [Ren83, Sul87] suggest that since the neutron spectrum in molasse is probably independent of position, a single number can be quoted representing the production probability of these nuclides. The activity of each nuclide after 10 years of operation can be calculated by estimating the activity produced each year and multiplying it by the appropriate decay factor. The acceptability of induced radioactivity in the rock could be judged by comparing the specific activities of the produced nuclides with the Exemption Limits (LE) of the Swiss legislation [ORaP]. It shall be noted that for a mixture of radionuclides, the value obtained with the additive rule given in Annex 1 of ref. [ORaP] should be smaller than 1. The specific activities of the most important radionuclides scored in the first 10 cm thick layer of rock after 10 years of operation (standard conditions) are shown in table 8.

Table 8. Specific activities (Bq g^{-1}) of the most important radioactive nuclides scored in the first layer of molasse after one year and ten years of operation, their saturation activities (Bq g^{-1}) and the Swiss Exemption limits (Bq g^{-1}).

Nuclide	$T_{1/2}$	1 year operation	10 year operation	Saturation	LE
^{3}H	12.4 y	4.4	34.6	57.8	200
^{7}Be	53.3 d	8.6	8.7	9.5	400
^{22}Na	2.6 y	4.4	17.4	34.9	3
^{45}Ca	163 d	10.3	13.1	19.1	10
^{46}Sc	83.8 d	1.2	1.3	1.6	7
^{54}Mn	313 d	4.2	7.6	12.7	10
^{60}Co	5.27 y	0.6	3.6	9.5	1
^{152}Eu	13.3 y	0.8	6.6	31.8	7
^{154}Eu	8.8	0.07	0.5	1.9	5

After 10 years of operation a 1.5 m thick layer of concrete and rock will have a radioactivity exceeding the Swiss Exemption limits. The number of years to wait before molasse could be considered as 'non-radioactive' is shown in figure 6 as a function of depth in the rock. Values referring to concrete were actually calculated assuming the same chemical composition of molasse, and are only given as a reference for thinner concrete layers.

The production of radioactive nuclides in the concrete wall of the decay ring, if suitably isolated, is of little consequence for the public water supplies, because the nuclides are relatively immobile. However, the radionuclides created in the rock could represent a danger, because they may leach into the ground water (indirect production) and transfer from the site of activation to the ground water table. Of all radioactive nuclides produced in the rock, it is likely that only ^{3}H will move freely in ground water without significant absorption on rock surfaces. However, ^{22}Na also has to be taken into account in assessing the contamination risk, because about 20% of its activity is produced in a chemical form that is extremely soluble in water [Tho88]. To this one must add the direct production of tritium by spallation reactions in the oxygen of the water, which can be estimated from the star density in the rock [Ste92] knowing that the interaction mean free path in water is approximately twice that in the rock and the proportion by volume of water in molasse is estimated to be 10% [Ste89].

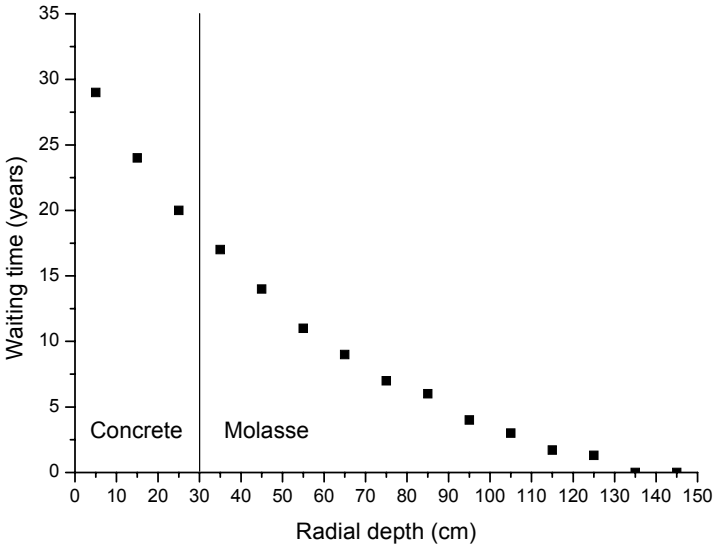

Figure 6. Waiting time (years) before the induced radioactivity in molasse decreases below the Swiss Exemption limit, as a function of depth in the concrete and rock.

The highest concentrations of ^{3}H and ^{22}Na produced in ground water (direct and indirect production) during operation are $7.4 \cdot 10^{-3}$ and $1.4 \cdot 10^{-3}$ Bq l^{-1} s^{-1}, respectively. These values may be used to estimate the highest concentration of radioactive nuclides that may be expected in the public water supply, once the site of the facility is known.

The models and scenarios for calculating the dose due to releases of radioactivity from nuclear installations, recommended in the Swiss directive HSK-R-41 [HSK97], were used by P. Vojtyla as guidelines for the calculation of the effective dose per unit release for long-term water releases for two critical groups (the so-called 'near' and 'far' groups) of the population located near the CERN area [Voj98]. From these data and from the annual releases of ^{3}H and ^{22}Na ($7.3 \cdot 10^{10}$ and $3.9 \cdot 10^{11}$ Bq, respectively) in the groundwater surrounding the arcs, it was possible to estimate the annual dose to the critical groups through the water pathway (table 9).

Table 9. Effective dose to the two critical groups of the population during one year of operation, water pathway (μSv per year). The effective dose limit for the public to which CERN adheres is 300 μSv per year [CERN96].

Effective dose, μSv per year	Near group	Far group
Infants	17	0.05
Adults	52	0.03
Total: 69.1		

8. Conclusions

The intention of this work was to obtain initial values of the parameters of radiological interest for the decay ring of a Beta-beam facility. Although there is still no detailed layout of the decay ring and the material activation strongly depends on the beam intensities and operation time, some preliminary conclusions can be drawn under the hypothesis made. In particular, it has been assumed that no material activation is expected from decay losses in the straight sections. The arcs are assumed to be 300 m in radius.

After 10 years of operation and 10 year decay time, magnets and vacuum chambers in the arcs still have a level of induced radioactivity exceeding the Swiss Exemption Limits and should be disposed of as radioactive waste.

The dose rate in contact with magnets in the arcs after 30 day operation and one day cooling is 2.5 mSv h^{-1}. Any maintenance operation in the arcs just after irradiation, if not remote-handled, must be carefully planned to reduce radiation exposure of personnel (High-radiation Area, >2 mSv h^{-1} [CERN96]). The dose rate in contact with magnets and vacuum chambers in the straight sections after 30 day operation and one day cooling is 0.4 μSv h^{-1}. This value is low enough for the tunnel to remain supervised area (<2.5 μSv h^{-1}), if magnets were to be the only radioactive components in the ring and beam-gas interactions the only source of radioactivity. However, it may be prudent to designate these parts of the ring as Controlled Radiation Areas (>2.5 μSv h^{-1}), in particular if decay losses will prove to give a non-negligible contribution to material activation also in the straight sections.

After 10 years of operation and one month decay time, the highest dose rate expected in the decay ring from magnets, vacuum chambers and concrete wall is 0.8 mSv h^{-1}. Arcs will still be designated as Limited-stay Areas and the access will have to be supervised by RP staff (Limited-stay Areas, >25 μSv h^{-1}).

After the final shutdown of the facility, the induced radioactivity in a 1.5 m thick layer of concrete and rock will be above the Swiss Exemption Limits. The induced radioactivity in ground water shall not represent a danger for the public, unless the site of construction of the facility is close to a public water supply.

References

[Ago01] S. Agosteo, C. Birattari, A. Foglio Para, M. Silari, L. Ulrici, *Neutron measurements around a beam dump bombarded by high energy protons and lead ions*, Nucl. Instr. and Meth. in Phys. Res., A 459 58-65 (2001).

[Ago02] S. Agosteo, C. Birattari, A. Foglio Para, L. Gini, A. Mitaroff, M. Silari, L. Ulrici, *Neutron production from 158 GeV/c per nucleon lead ions on thin copper and lead targets in the angular range 30-135 degree*, Nucl. Instr. and Meth. in Phys. Res., B 194 399-408 (2002).

[And02] V. Andersen et al., *The FLUKA code for space applications: recent developments*, Proceedings of the 34th COSPAR scientific assembly, World Space Congress, 10-19 October 2002, Houston, Texas, USA (2002).

[Bon02] K. Bongardt, F. Caspers, H. Frischholz, F. Gerigk, A.M. Lombardi, R. Losito, A. Mostacci, M. Paoluzzi, J. Tückmantel, M. Vretenar, *Progress in the design of the SPL, an H⁻ high-intensity linac at CERN*, CERN-SL-2002-027 (2002).

[CERN96] CERN Radiation Safety Manual (1996).

[Fas00a] A. Fassò, A. Ferrari and P.R. Sala, *Electron-photon transport in FLUKA: status*, Proc. of the MonteCarlo 2000 Conference, Lisbon, October 23-26, 2000, A. Kling, F. Barao, M. Nakagawa, L. Tavora, P. Vaz – eds., Springer-Verlag Berlin, 159-164 (2001).

[Fas00b] A. Fassò, A. Ferrari, J. Ranft and P.R. Sala, *FLUKA: Status and prospective for hadronic applications*, Proc. of the MonteCarlo 2000 Conference, Lisbon, October 23-26 2000, A. Kling, F. Barao, M. Nakagawa, L. Tavora, P. Vaz – eds., Springer-Verlag Berlin 955-960 (2001).

[Hoe75] M. Hoefert and A. Bonifas, *Measurement of radiation parameters for the prediction of dose-rates from induced radioactivity*, CERN/HP-75-148 (1975).

[HSK97] *Hauptabteilung für Sicherheit der Kernanlangen (HSK), Berechnung der Strahlenexposition in der Umgebung aufgrund von Emissionen radioactiver Stoffe aus Kernanlangen*, HSK-R-41/d (1997).

[Jan03] A. Jansson, *Private communication* (2003).

[Lin02] M. Lindroos et al., *The acceleration and storage of radioactive ions for Neutrino Factory*, CERN/PS-2002-078 (2002).

[Lin03] M. Lindroos, *Private communication* (2003).

[Mic96] MicroShield Version 5, Grove Engineering, Rockville, Maryland, USA.

[Mok98] N.V. Mokhov, S.I. Striganov, A. Van Ginneken, S.G. Mashnik, A.J. Sierk and J. Ranft, *MARS code developments*, Proceedings of the Fourth Workshop on Simulating Accelerator Radiation Environments (SARE4), Knoxville (TN, USA), 14-16 September 1998, Ed. T. Gabriel, ORNL 87-99 (1998).

[ORaP] *Ordonnance sur la radioprotection (ORaP) du 22 juin 1994* (Etat le 4 avril 2000).

[Pra89] R.E. Prael and H. Lichtenstein, *User guide to LCS: The LAHET Code System*, LA-UR-89-3014, Los Alamos National Laboratory, Los Alamos, New Mexico (1989).

[Ren83] C. Renaud et A.H. Sullivan, *Démantèlement d`un tunnel utilisé comme blindage pour un faisceau de protons à haute énergie*, Rayonnements Ionisants 26 (1983) 4.

[Ste89] G.R Stevenson and R.H. Thomas, *Radiological considerations for the environment around the LHC*, Minutes of a Workshop, 22-26th May 1989, CERN-TIS/89-19 (LHC Note 115) (1989).

[Ste92] G.R. Stevenson, A. Fassò and J.M. Zazula, *The estimation of parameters of radiological interest for the LHC main ring*, CERN/TIS-RP/IR/92-08 (1992).

[Sul87] A.H. Sullivan, *Ground activation around the AA and ACOL target areas*, Internal Report CERN TIS-RP/IR/87-34 (1987).

[Tho88] R.H. Thomas and G.R. Stevenson, *Radiological safety aspects of the operation of proton accelerators*, International Atomic Energy Agency, Technical Reports Series n. 283, Vienna (1988).

[Voj98] P. Vojtyla, *Calculation of the effective dose to the public due to releases from the CERN Meyrin site implementing the Swiss directive HSK-R-41*, CERN/TIS-TE/98-20 (1998).